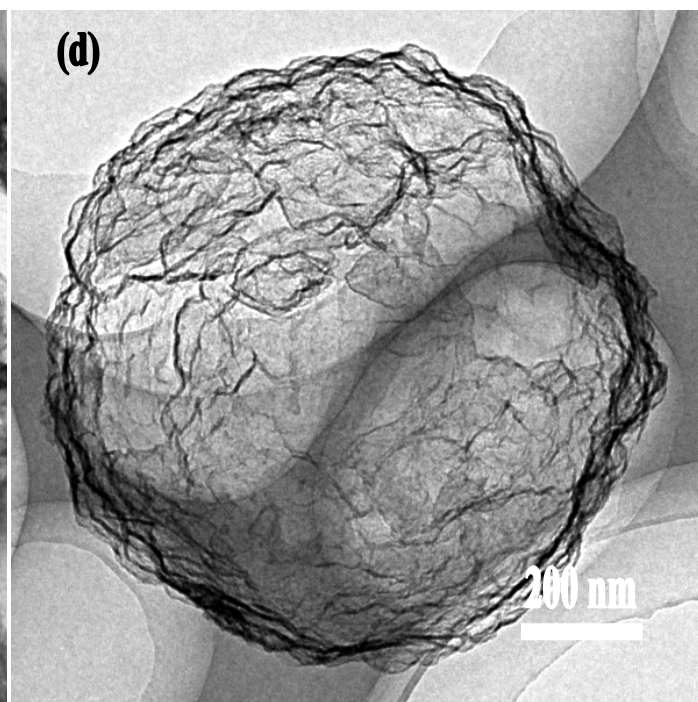
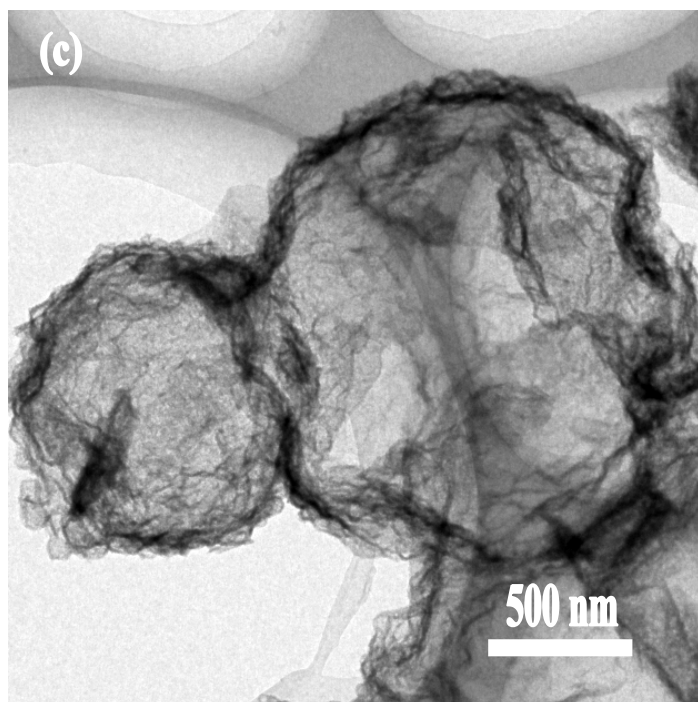
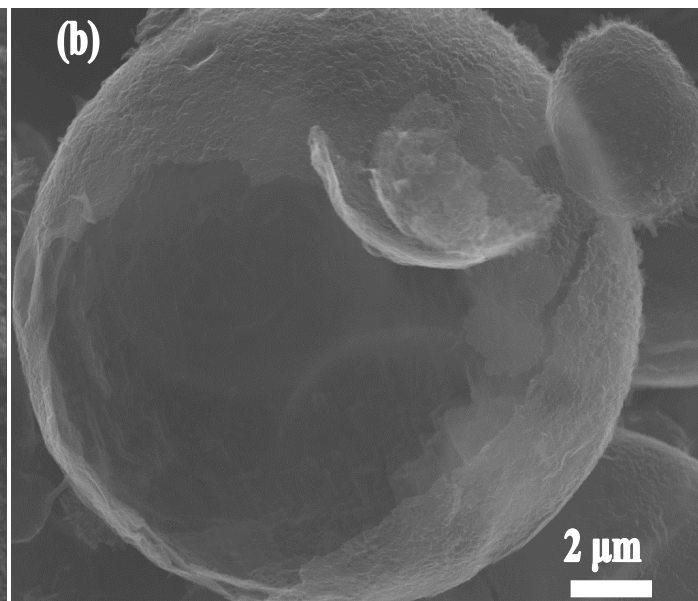
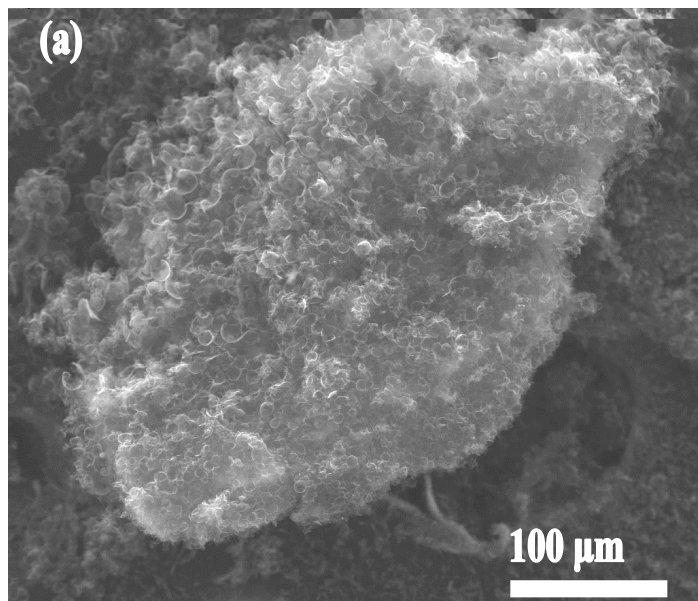


Supporting Information



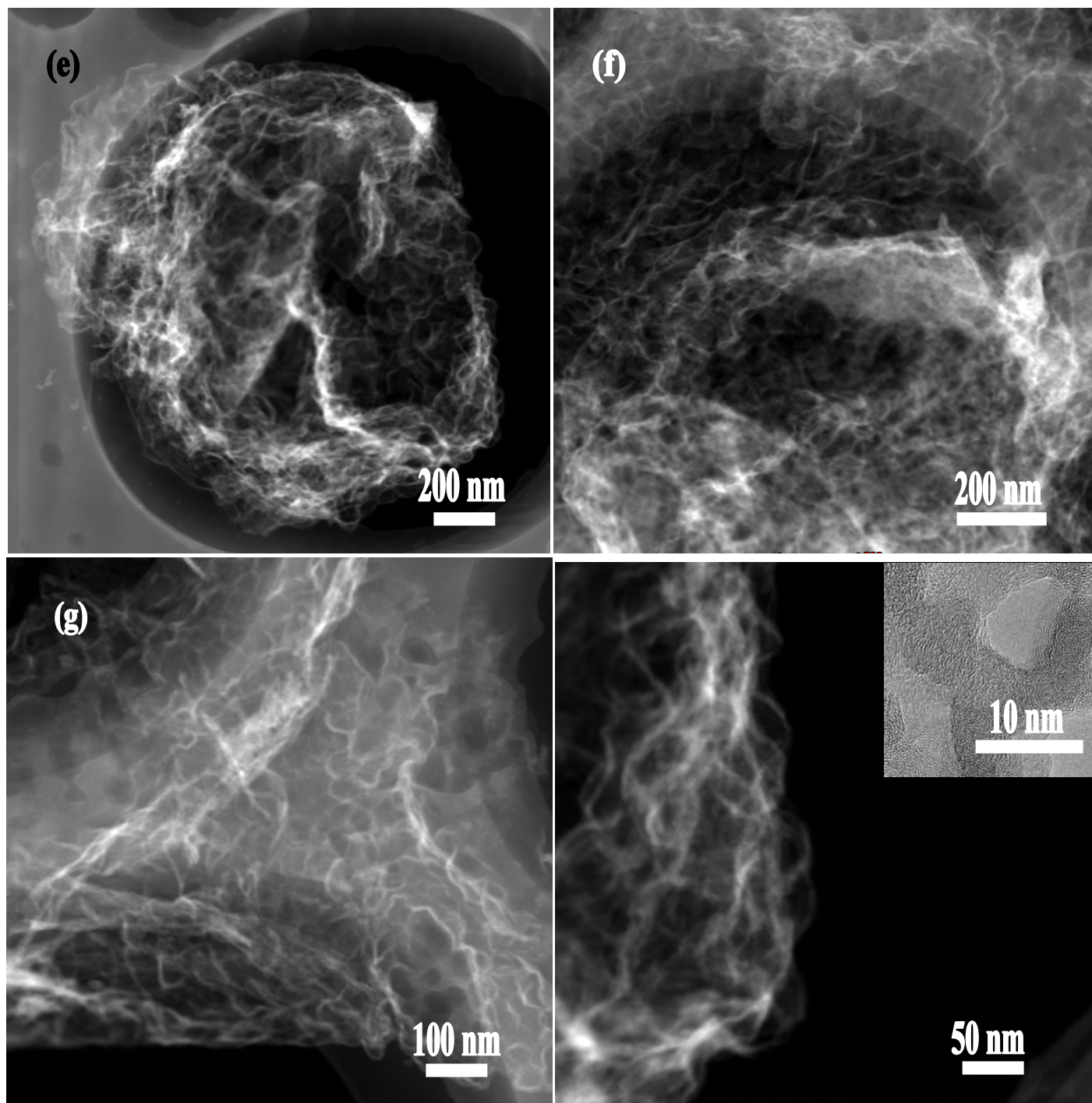


Figure S1 (a) and (b) SEM images, (c) and (d) TEM images, and (e-g) STEM images showing the honeycomb-like CMBs characteristic of small porous nests in the shell; (h) a STEM side view for the shell of the CMBs with HRTEM in the inset view showing its porous and partial graphitized structure.

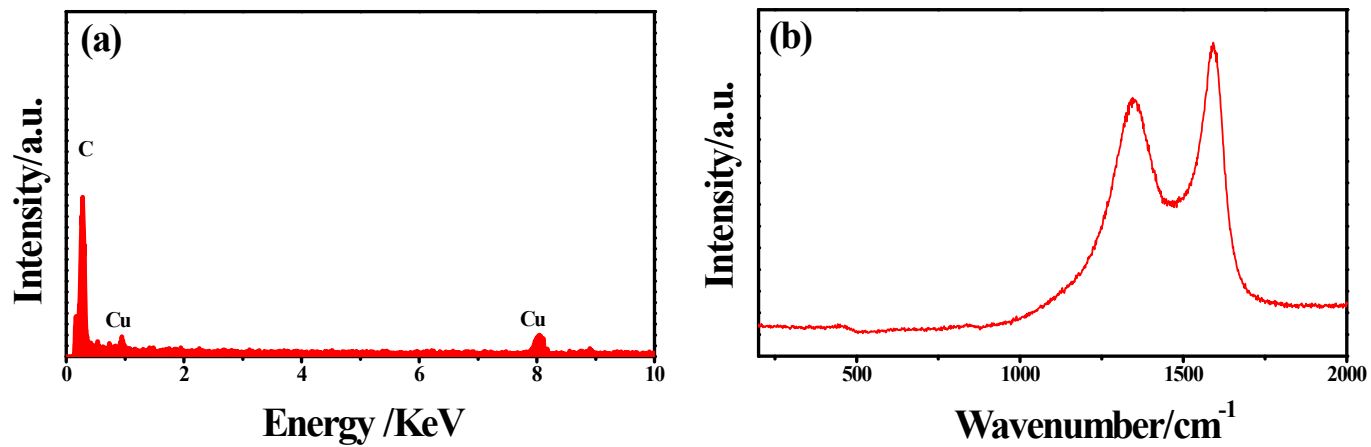


Figure S2 (a) EDS and (b) Raman spectra for the porous honeycomb-like CMBs showing the carbon nanostructures are partial graphitized.

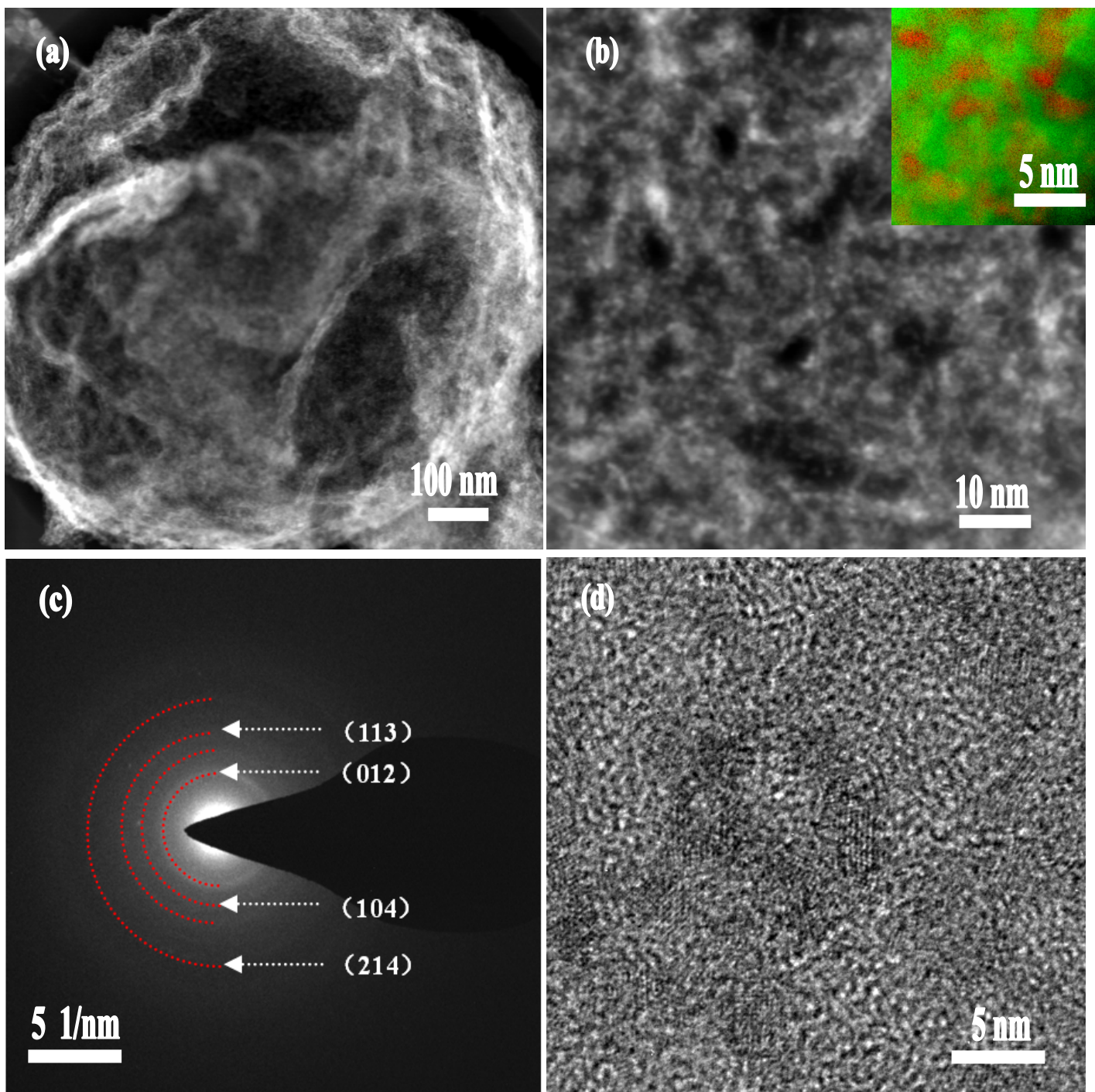


Figure S3 Microstructures for IOCMBs: (a) and (b) STEM images with Fe mapping in red and C mapping in green (inset view of (b)) showing uniformly distributed iron oxide nanoparticles intimately encapsulated in the honeycomb-like CMBs; (c) SAED image implies these iron oxide particles are well consistent with rhombohedral Fe_2O_3 (R- Fe_2O_3 , space group: R-3c(167), $a=b=5.0356$, $c=13.7489$, $\alpha=\beta=90^\circ$, $\gamma=120^\circ$) in structure; (d) HRTEM image showing nanocrystals of iron oxide have small size of ~ 2 nm.

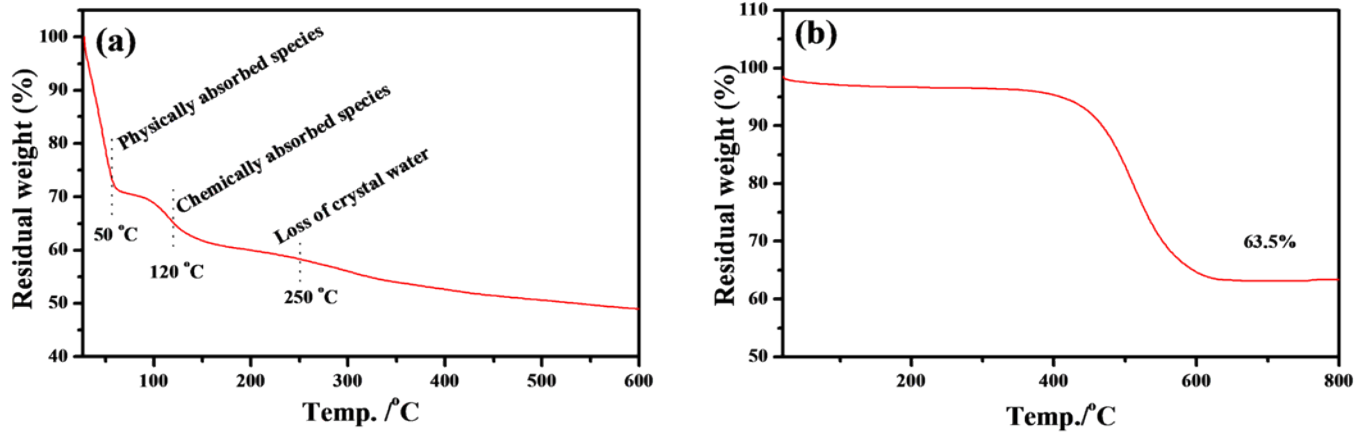


Figure S4 TG curves of (a) the fluorinated IOCMBs precursor sweep from room temperature to 600 °C with a ramp rate of 5 °C/min under N₂ atmosphere and (b) the IFCMBs hybrid composites recording from room temperature to 800 °C with a ramp rate of 10 °C/min at ambient atmosphere.

Analysis of TG curves

As shown in Figure S4 (a), the fluorinated IOCMBs precursor suffers three sections of mass loss when annealing in N₂ atmosphere. The first decrease around 50 °C probably results from the loss of weak physical absorbed HF or H₂O atoms; when the heating temperature increases, the chemically absorbed species begin to be removed about 120 °C; the final decrease around 250 °C may be assigned to the loss of crystal water. In the IFCMBs hybrid, FeF_x will be transformed into Fe₂O₃ at high temperature in O₂ atmosphere. According to Figure S4 (b), the FeF_x has a weight proportion about 71% in the composite.

The weight proportion (WP) for FeF_x in the composite is deduced from the follow equation:

$$WP_{FeF_x} = \frac{(2 \cdot 0.635 / M_{Fe_2O_3}) \cdot M_{FeF_x}}{[(2 \cdot 0.635 / M_{Fe_2O_3}) \cdot M_{FeF_x} + 0.365]}$$

$$M_{Fe_2O_3}$$
 and M_{FeF_x} are relative molecular weight for Fe₂O₃ and FeF_x respectively, and 0.635 is the residual weight obtained from Figure S4 (b).

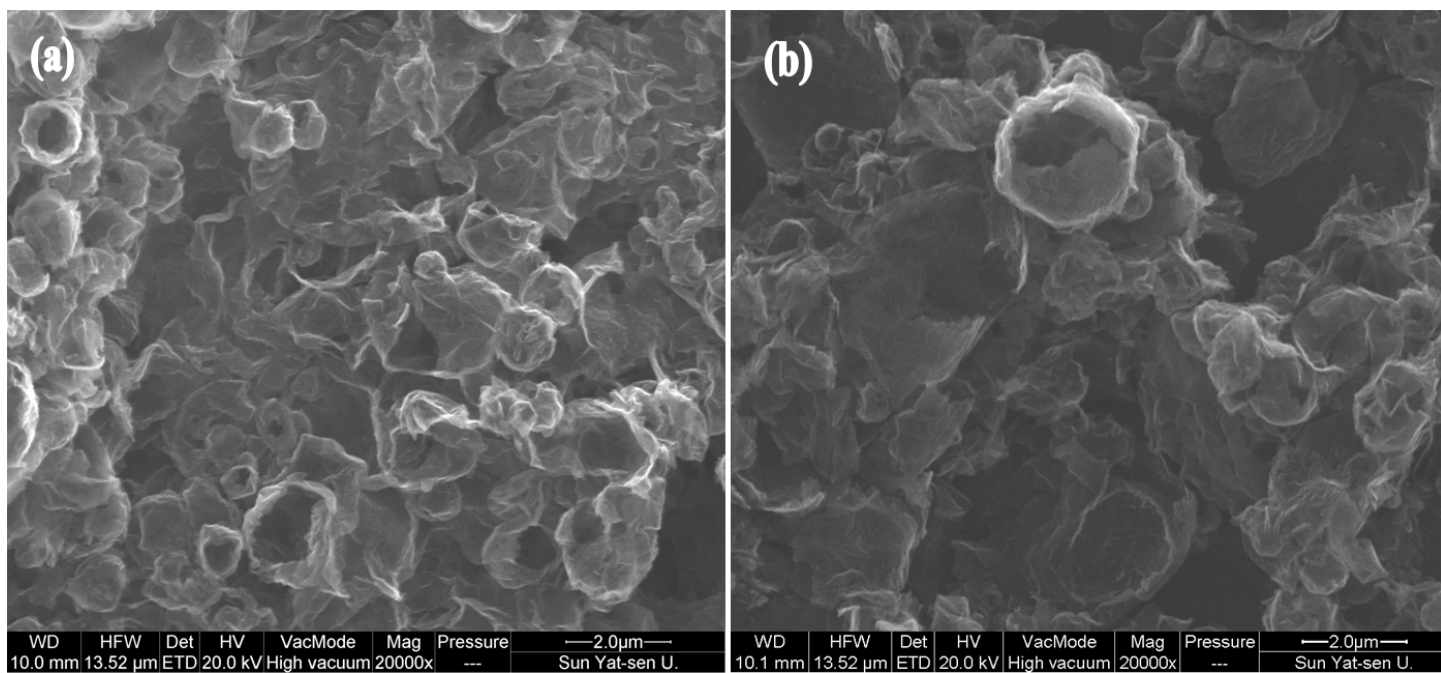


Figure S5 SEM images showing porous (a) IOCMBs precursor and (b) IFCMBs without any iron oxide or iron fluoride agglomerates.

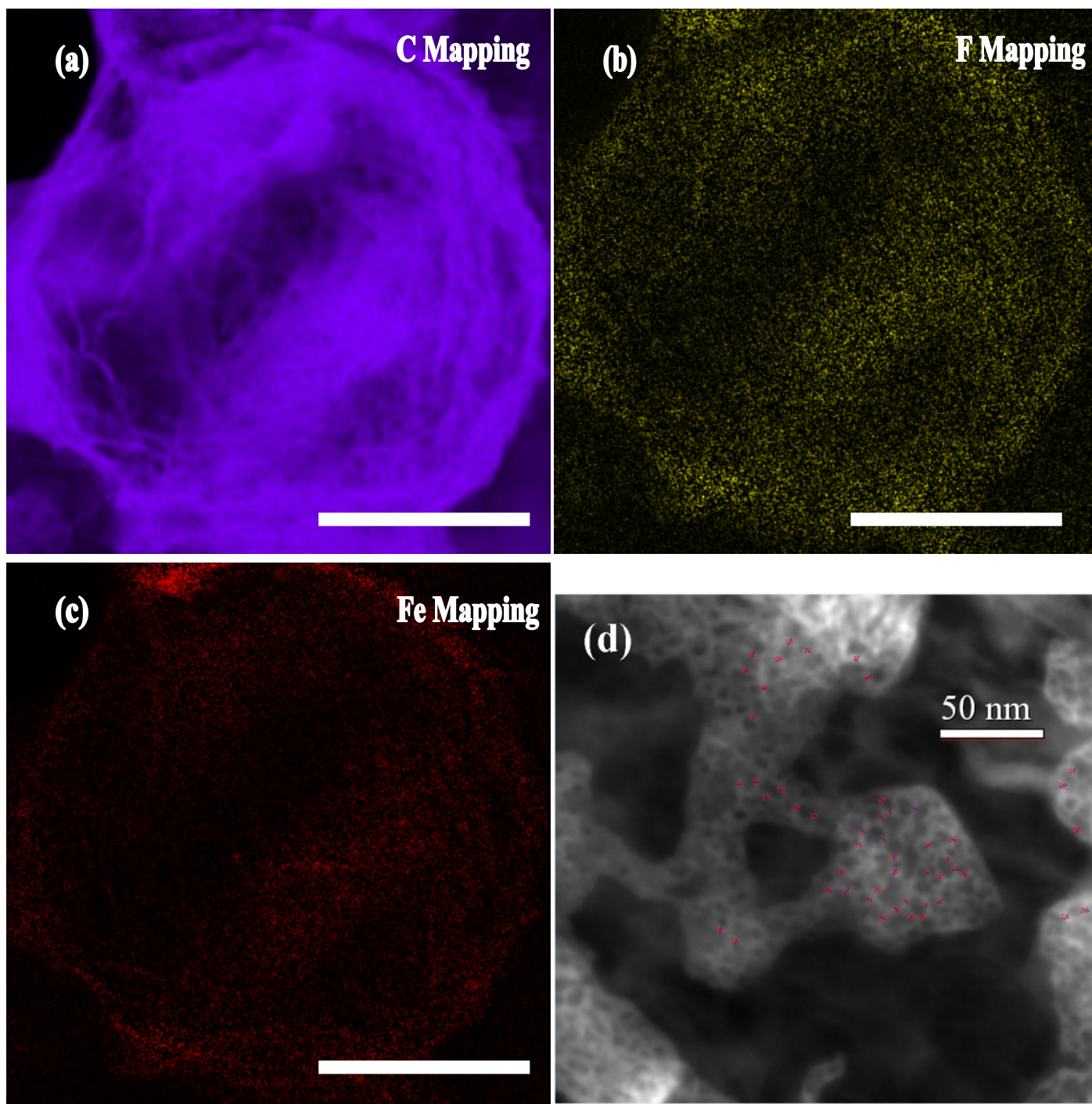


Figure S6 (a-c)Element mapping images for IFCMBs showing Fe, F uniformly distributed in the honeycomb-like porous CMBs, the scale bars are 500 nm; (d) presents labeled walls for the honeycomb-like porous IFCMBs for evaluation in the size of the iron fluoride nanostructures.

Table S1 Thicknesses for the randomly labeled wall nested in IFCMBs hybrid composite.

No.	Thickness/nm								
1	2.95	11	2.24	21	2.64	31	3.11	41	4.17
2	3.20	12	1.76	22	3.12	32	2.09	42	3.11
3	2.64	13	1.76	23	3.47	33	2.51	43	3.06
4	1.96	14	2.20	24	3.06	34	2.43	44	2.51
5	2.51	15	2.86	25	3.85	35	2.78	45	2.17
6	2.50	16	2.56	26	2.37	36	2.51	46	2.95
7	1.99	17	2.78	27	2.20	37	2.81	47	2.82
8	1.58	18	2.87	28	2.64	38	2.49	48	3.47
9	1.55	19	3.64	29	2.56	39	3.76	49	2.08
10	2.24	20	2.50	30	2.78	40	3.06	50	3.08

Table S2 Statistics information for the thicknesses in Table S1.

Distribution for thickness	Mean thickness/nm	Counts
1-1.4	1.2	0
1.4-1.8	1.6	4
1.8-2.2	2	5
2.2-2.6	2.4	15
2.6-3	2.8	12
3-3.4	3.2	8
3.4-3.8	3.6	4
3.8-4.2	4	2
4.2-4.6	4.4	0
4.6-5	4.8	0

Table S3 Specific lattice planes and their corresponding $2\langle\theta\rangle$ and d-spacing survey for LiF (Space group:Fm-3m (225)), γ -Fe (Space group: Fm-3m (225)), and $\text{Li}_x\text{FeF}_{3+y}$ ($x=y=3$, Space group: Pna21(33)).

LiF	γ -Fe	$\text{Li}_x\text{FeF}_{3+y}$ ($x=y=3$)
		(210)-21.1°-0.419nm
(111)-38.7°-0.232nm	(111)-42.7°-0.211nm	(310)-29.6°-0.301nm
(200)-44.9°-0.201nm	(200)-49.8°-0.183nm	(221)-33.3°-0.268nm
(220)-65.5°-0.142nm	(220)-73.1°-0.129nm	(212)-41.9°-0.215nm
(311)-78.8°-0.121nm	(311)-88.5°-0.110nm	(422)-57.3°-0.161nm
		(432)-62.7°-0.148nm

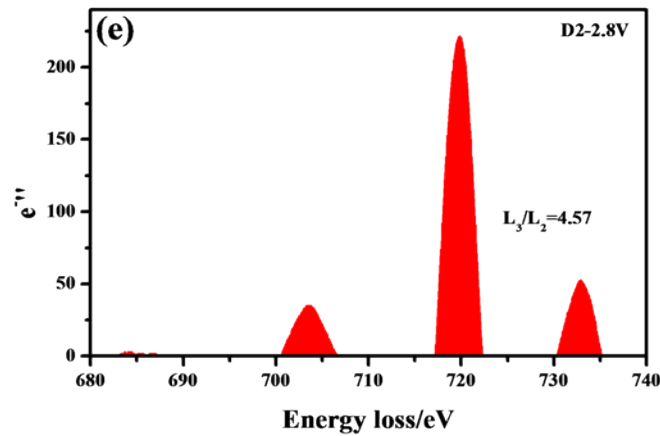
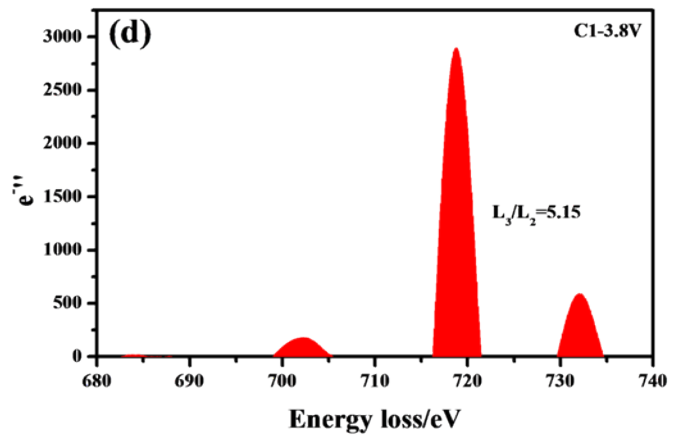
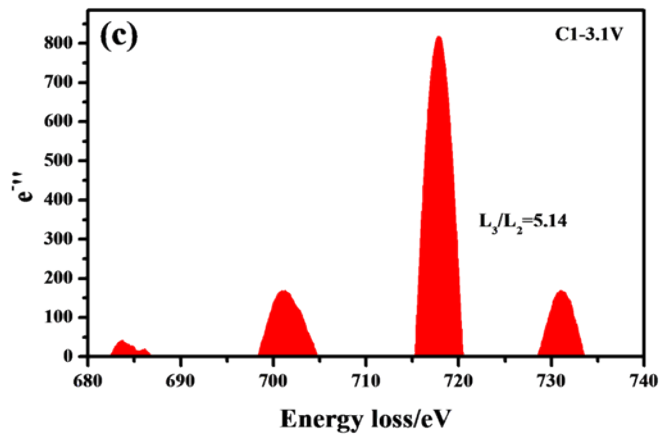
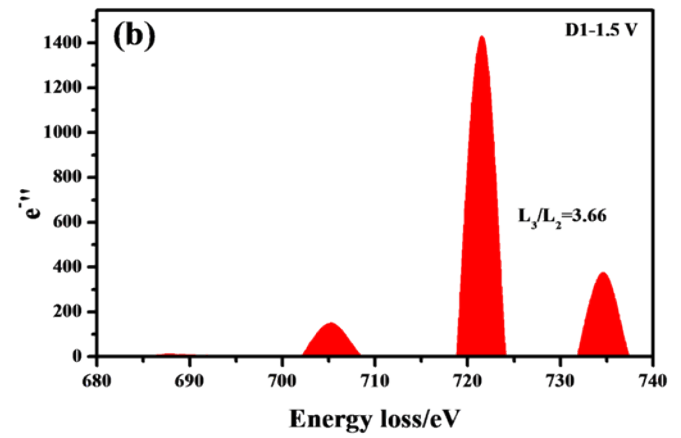
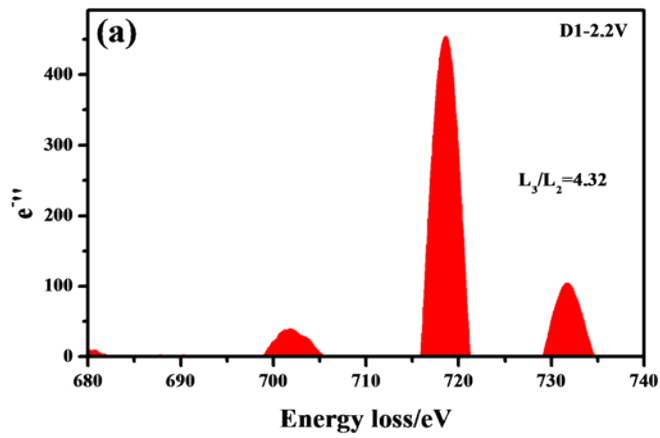


Figure S7 The second derivative for the positive intensity of the deconvoluted EELS spectra at different cutoff voltages.

